13th International Symposium on Particle Image Velocimetry – ISPIV 2019
Munich, Germany, July 22-24, 2019

RainbowPIV with Improved Depth Resolution – Design and Comparative Study with TomoPIV

Jinhui Xiong[1], Andres A. Aguirre-Pablo[2], Ramzi Idoughi[1], Sigurdur T. Thoroddsen[2], Wolfgang Heidrich [1*]

[1] King Abdullah University of Science and Technology (KAUST), Computer Science and Visual Computing Center, Thuwal, Saudi Arabia

[2] King Abdullah University of Science and Technology (KAUST), Mechanical Engineering, Thuwal, Saudi Arabia

[*] wolfgang.heidrich@kaust.edu.sa

Abstract

RainbowPIV is a recent imaging technology proposed for time-resolved 3D-3C fluid velocity measurement using a single RGB camera. It dramatically simplifies the hardware setup and calibration procedures required compared to alternative 3D-3C measurement approaches. RainbowPIV combines optical design and tailored reconstruction algorithms, and preliminarily studies demonstrated its ability to extract physically constrained fluid vector fields. This article addresses the issue of limited axial resolution, the major drawback of the original RainbowPIV system. We validate the new system with a direct, quantitative comparison to four-camera Tomo-PIV. The reconstructed flow vectors of the two approaches exhibit a high degree of consistency, with the RainbowPIV results explicitly guaranteeing physical properties such as divergence free velocity fields for incompressible fluid flows.

1 Introduction

In recent years, a great amount of effort has been invested into the development of methods for complete volumetric reconstruction of the three-dimensional, three-component (3D-3C) velocity vector fields. Tomographic Particle Imaging Velocimetry (Tomo-PIV) (Elsinga et al., 2006; Scarano, 2012) has long been considered as the standard technology for 3D measurement owing to its capability to handle high particle seeding densities and high spatial resolution reconstruction, as well as its robustness to many types of the flow phenomena. Most recent advances regarding Tomo-PIV have been carried out for improving reconstruction accuracy (Schanz et al., 2016) or spatial and temporal resolution (Scarano and Moore, 2012; Schneiders and Scarano, 2016) by exploiting temporal coherence, or reducing the cost of the setup, e.g. using smartphones (Aguirre-Pablo et al., 2017; Cierpka et al., 2016). Tomo-PIV typically makes use of 4-6 cameras capturing the volume of interest from different viewing angles. While Tomo-PIV has the abovementioned advantages, it also suffers from several limitations that constrain its use. First, a considerable amount of effort is required to set up and calibrate a multi-camera system. Precise calibration is required, otherwise, calibration error may result in a degradation on the reconstruction quality. Depth-of-the-field is another practical issue that Tomo-PIV, in general, cannot be applied for relatively large-scale fluid measurement applications. A more severe limitation is that there are many experimental setups where optical access is limited, and thus setting up a multi-camera system becomes impractical. In such situation, a single-camera based 3D-3C technology would be desired.

There are mainly two types of single-camera approaches proposed in the last decades for 3D flow measurement, specifically, encoding the particle depth by light path in the camera side or by color or spectral information in the illumination side. The strategy of encoding the particle depth by light path dates back to the work of Willert et al. (Willert and Gharib, 1992), which attaches a three-pin-hole mask in front of the objective, and recover the 3D particle locations based on the position and length of the captured image patterns (equilateral triangle) by means of defocusing technique. This method has been applied to several flow scenarios (Pereira and Gharib, 2002; Yoon and Kim, 2006), although it has the disadvantages of low

light efficiency due to the fact that not the whole apertures (only three pinholes) are utilized and low particle seeding density because of the ambiguity to distinguish overlapped image patterns for neighbor particles. More recently, plenoptic camera (or light-field camera) based single-camera PIV approaches have been proposed in (Fahringer et al., 2015; Shi et al., 2016), which records the full 4D light field of the scattered light of the seeding particles and digitally reconstructs particle locations by means of ray-tracing based algorithms. Quantitative comparisons between Tomo-PIV and Plenoptic-PIV have been conducted in recent work (Shi et al., 2018; Rice et al., 2018). Plenoptic-PIV dramatically simplifies the hardware setup and gets rid of the complicated calibration procedures required in Tomo-PIV, while as a compromise, the spatial resolution is significantly sacrificed for the angular information to achieve desired depth resolution. Besides, the plenoptic camera normally has low frame rate, which restricts its usage for time-resolved non-stationary fluid flow measurements.

Another group of single-camera methods is based on the encoding of the particle depth by structured light (monochromatic or polychromatic light), thus the 3D particle locations can be determined by 2D spatial location and 1D light illuminated information in the captured single image. The method of exploiting monochromatic illumination has been proposed in (Aguirre-Pablo et al., 2019), which illuminates the volume by a spatially and temporally varying intensity profiles and achieves 200-levels depth resolution. However, the temporal resolution is sacrificed in a certain extend for the sake of high depth resolution, and also it fails to separate overlapped particles. Most of the related work using polychromatic illumination is summarized in (Watamura et al., 2013). Early work extracts the particle depth based on a calibrated mapping function of RGB or hue value to depth. This naive method cannot deal with overlapping particles, and thus it is not suitable for dense fluid flow reconstructions. An additional disadvantage is that the method is sensitive to random noise, optical aberration and unpredictable secondary light scattering from the particles. Recently proposed RainbowPIV (Xiong et al., 2017) tackles most of the existing issues by a combinational design of the illumination and optics, in conjunction with an integrated optimization framework to jointly reconstruct both of the particle distribution fields and velocity vector fields. While it suffers from a limited and fixed volume size due to the rainbow generation engine (linear variable filter) and the constant focal length of the specifically designed optics (diffractive optical elements). Xiong et al. (Xiong et al., 2018) further proposed a reconfigurable RainbowPIV system with an adjustable rainbow generation engine and a varifocal optical design, extending it to a volume size with a considerable range.

Even though these single-camera approaches achieved by color-encoded illumination greatly simplify the hardware setup with respect to both Tomo-PIV and Plenoptic-PIV, and significant improvements have been made recently for 3D dense fluid velocity imaging, the limited axial resolution is still a major drawback for this type of method, which constrains its usage in fluid measurement applications requiring a high depth resolution. In this work, we address this issue and propose an extension to the precedent RainbowPIV, implementing a depth super-resolved RainbowPIV system. Furthermore, we carry out a direct comparison with the well established four-camera Tomo-PIV system to verify its applicability and reconstruction accuracy for flow measurement. Moreover, we demonstrate that RainbowPIV, unlike Tomo-PIV, reconstructs physically plausible flows e.g. divergence free flow fields in the case of incompressible fluid flow.

2 System Overview

In order to realize a simultaneous measurement with RainbowPIV and Tomo-PIV, the schematic diagram for the designed experimental setup is shown in Fig. 1. Four cameras are arranged to view the octagonal tank from different perspectives for Tomo-PIV. Among these, the central camera, equipped with a specially designed diffractive optical element (DOE) and achieving a hybrid refractive/diffractive imaging system, is also utilized for RainbowPIV. All cameras are triggered by a synchronized signal. The DOE is a Fresnel phase plate used for all-in-focus imaging in the RainbowPIV setup. Normally, the cameras used in Tomo-PIV setup keep a relatively small aperture size for a large depth-of-field, in the meantime, the light efficiency is reduced proportional to the inverse of the square of the F-number (smaller aperture size means lower light efficiency). In contrast, the depth-of-field of the utilized hybrid refractive/diffractive lens is not affected by the aperture size, hence RainbowPIV can make use of the largest available aperture for maximum light efficiency, and still maintain an extended depth-of-field. The design, fabrication and impact of the DOE are explained in detail in (Xiong et al., 2017).

Another notable part is the illumination system (rainbow generation). The physical size of the measured volume is dependent on the field-of-view of the camera (x-y) and the illumination width (z), corresponding to the rainbow width. In order to generate parallel and size-controlled rainbow, we utilize two blazed gratings and place them parallel to each other at the blazed angle. With a while light beam comes in, output of this

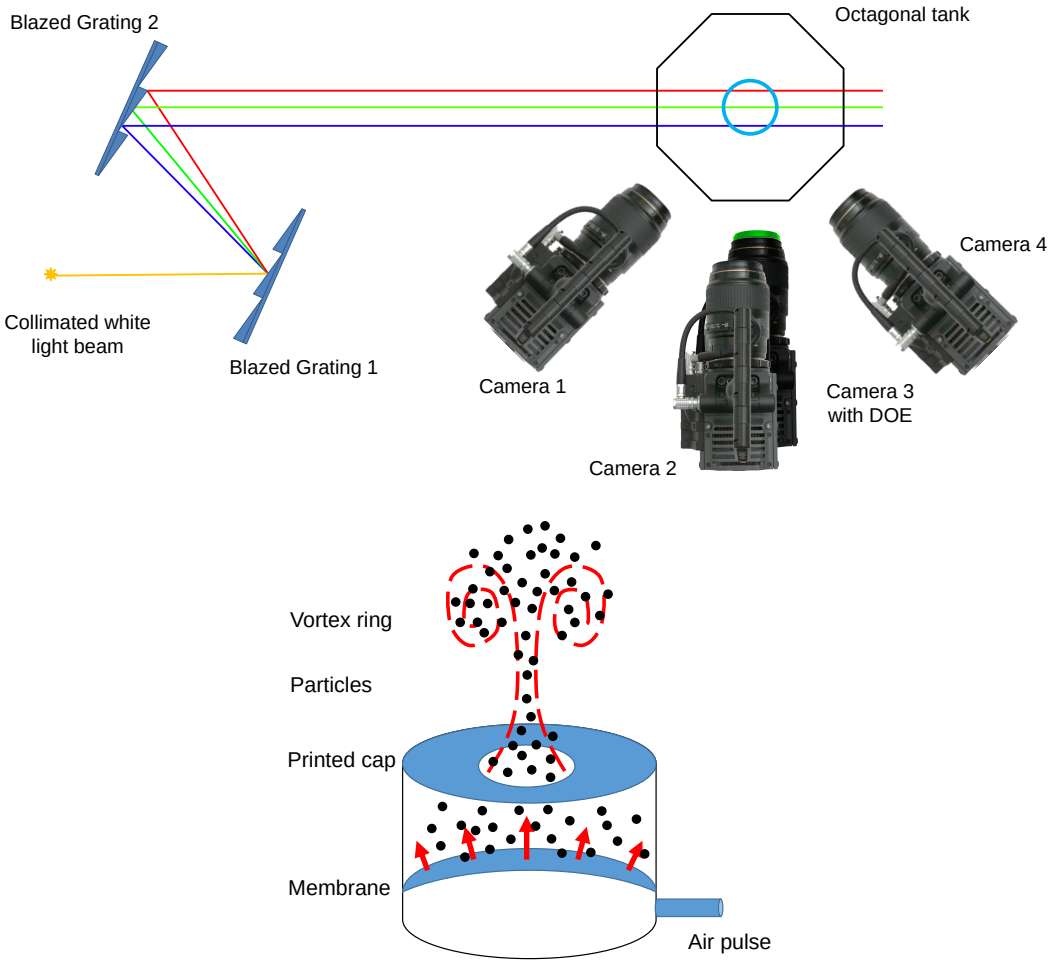

Figure 1: Schematic diagram for the experimental setup (top) and the vortex ring generator (bottom). Two blazed gratings are utilized for generating size-controlled rainbow. Four cameras are utilized for Tomo-PIV measurement, among which, the third camera with custom designed DOE is also used for RainbowPIV. Instead of multiple optical access points to the measured volume required by the Tomo-PIV system, RainbowPIV requires only one camera and one illumination access port.

system is a parallel rainbow, the size of which can be adjusted by altering the distance between these two gratings.

We place a vortex ring generator (Fig. 1) beneath the tank to produce specific flow scenarios for measurements. Specifically, it is composed of a circular chamber covered by an elastic latex membrane. The whole is then enclosed by a 3D printed cap with a small circular centered hole on the top. The air pulse comes into the chamber and upwards pressurizes the membrane, driving the water pass through the membrane and the hole on the cap, finally generates the desired vortex ring.

3 RainbowPIV Tracking and Reconstruction

3.1 Joint Optimization Framework

In order to fully reconstruct the dense 3D-3C velocity fields, prior work utilizes a pipeline approach that firstly estimates the particle distribution fields at successive time steps, and then reconstructs the corresponding flow fields using the estimated particle distributions. Such a pipeline approach neglects strong physical cues for temporal coherence, which can significantly improve the results. Specifically, particles

present at current time step should also be present at the subsequent time step and the previous time step as well (excluding a small number of disappeared and new-coming particles), and their location should be consistent with the estimated 3D-3C flow fields. RainbowPIV, for the first time, proposed a joint optimization framework for particle distribution fields and fluid velocity vector fields reconstruction on a sequentially captured video frames. As illustrated in (Xiong et al., 2017), one can benefit from this prior information to refine those ambiguity particles computed from a single frame, obtaining more precise flow fields. This joint optimization framework has also been utilized for multi-camera 3D Fluid Flow Estimation (Lasinger et al., 2018) and X-ray computed tomographic applications (Zang et al., 2018), and exhibits improved reconstruction quality in respective work. Specifically, the integrated optimization problem for RainbowPIV can be expressed as:

$$
\begin{aligned}
(\mathbf{p}^*, \mathbf{u}^*) = \underset{\mathbf{p},\mathbf{u}}{\operatorname{argmin}} \ & \frac{1}{2} \left\| \mathbf{A} \left[\mathbf{p}_1 | ... | \mathbf{p}_\mathrm{T} \right] - \left[\mathbf{i}_1 | ... | \mathbf{i}_\mathrm{T} \right] \right\|_2^2 \\
& + \kappa_1 \left\| diag(\mathbf{w}) \left(\mathbf{p}_1; ...; \mathbf{p}_\mathrm{T} \right) \right\|_1 \ + \ \Pi_{[0,1]} \left(\mathbf{p}_1; ...; \mathbf{p}_\mathrm{T} \right) \\
& + \kappa_2 \sum_{\mathrm{t}=1}^{T} \int_\Omega \left(\mathbf{p}_\mathrm{t} - \mathbf{p}_{\mathrm{t}+1}(\mathbf{u}_\mathrm{t}, -\Delta t) \right)^{\circ 2} d\Omega \ + \ \kappa_3 \sum_{\mathrm{t}=1}^{T} \left\| \nabla \mathbf{u}_\mathrm{t} \right\|_2^2 \ + \ \sum_{\mathrm{t}=1}^{T} \Pi_{\mathcal{C}_\mathrm{DIV}} (\mathbf{u}_\mathrm{t}) \\
& + \kappa_4 \sum_{\mathrm{t}=1}^{T} \Big(\left\| \mathbf{u}_\mathrm{t} - \Pi_{\mathcal{C}_\mathrm{DIV}} (\mathbf{u}_{\mathrm{t}-1}(\mathbf{u}_{\mathrm{t}-1}, \Delta t)) \right\|_2^2 + \left\| \mathbf{u}_\mathrm{t} - \Pi_{\mathcal{C}_\mathrm{DIV}} (\mathbf{u}_{\mathrm{t}+1}(\mathbf{u}_\mathrm{t}, -\Delta t)) \right\|_2^2 \Big),
\end{aligned}
\tag{1}
$$

where $\mathbf{p}^*$ and $\mathbf{u}^*$ are the target particle distribution fields and fluid velocity vector fields, respectively. The above energy function is minimized using a coordinate decent method, alternating on these two variables. Specifically, we alternate between keeping $\mathbf{u}$ fixed, and solve for $\mathbf{p}$, and then fixing $\mathbf{p}$ and solving for $\mathbf{u}$. The following sections will provide intuitive motivations and explanations for the above optimization problem. More detailed derivations and solvers for it can be found in (Xiong et al., 2017).

3.2 Particle Distribution and Velocity Field Reconstruction

Starting with extracting the particle distributions from a single RGB image, straightforward ways have been proposed in (Watamura et al., 2013; McGregor et al., 2007), which relates the hue values of the captured image to the particle depth in the volume. This type of approach, as discussed before, cannot correctly extract the locations of overlapped particles due to the color mixing, also it is not robust to random noise and unpredictable light scattering occurred during the imaging and light propagation processes.

The above problem, alternatively, can be formulated as an inverse problem, and we can then efficiently and accurately solve it by exploiting modern optimization frameworks. Each possible particle in the 3D volume can be considered as a point light source, and the camera response to the point source is a point spread function (PSF), which is depth dependent. In order to construct the inverse problem, we first express the imaging system by a forward model, which is a linear process and can be expressed by $\mathbf{A}\mathbf{p}_\mathrm{t}$, with $\mathbf{A}$ being the coefficient matrix representing the convolution operation (with various PSFs) and $\mathbf{p}_\mathrm{t}$ being the particle distribution fields at time step t $(1 \leq t \leq T)$. Denoting the corresponding captured image as $\mathbf{i}_\mathrm{t}$, ideally, we have $\mathbf{A}\mathbf{p}_\mathrm{t} = \mathbf{i}_\mathrm{t}$.

However, this linear system is underdetermined (or ill-posed) since we have less constraints than unknown variables. Introducing additional regularization terms and constructing a minimization problem are common strategies to tackle this kind of problem. A sparse distribution of particles in the volume is expected (only a small percentage of voxels contains particles), and the value of the particle distribution fields should be within the range of 0 and 1. These two constraints account for the second and third terms in line 2 of Eq. (1), where $\| \cdot \|_1$ is the L_1 norm, κ_1 is the penalty parameter enforcing the sparsity. $diag(\mathbf{w})$ is the weights compensating the sensor sensitivity to different wavelengths, detailed explanation of which can be found in (Xiong et al., 2018). $\Pi_{[0,1]}$ is the operator projecting the value to the convex set $[0,1]$.

We can also take the temporal priors into account to alleviate the ambiguity of determining the particle distributions from sole image. The fourth term in the third line of Eq. (1), named as particle presence consistency, interprets the temporal coherence into the minimization problem, where $\mathbf{p}_{\mathrm{t}+1}(\mathbf{u}_\mathrm{t}, -\Delta t)$ indicates advecting the particle distribution fields at time step $t+1$ under flow field $\mathbf{u}_\mathrm{t}$ by $-\Delta t$ unit of time. Notice that this term is also used by reconstructing velocity fields.

After obtaining the particle fields in sequential time steps, we can then perform velocity estimation on them to generate the time-resolved velocity fields. A common method for such velocity estimation

methods is Digital Volume Correlation (DVC), based on cross-correlation of volume neighborhoods, or windows (Prasad, 2000). However, the window size can be difficult to choose, since large windows result in overly smooth flow fields, while small windows give wrong matches, especially on noisy low-light images. Furthermore, such algorithm requires a sufficiently high density of particles, which cannot always be satisfied in various flow scenarios, especially in 3D measurements. Moreover, the cross-correlation based framework does not easily support adding extra physical constraints, such as divergence free flows in the case of incompressible fluids.

An alternative method is adopted from the computer vision community, which solves a variational "optical flow" problem (corresponding to 2D digital image correlation), by finding the correspondence between two successive particle distribution fields. Liu et al. (Liu and Shen, 2008; Liu et al., 2015) first studied the connections between the optical flow and the fluid flow. Horn-Schunck algorithm is the most widely used global variational optical flow method, which assumes the brightness constancy between successive images and the smoothness of the flow vectors in spatial domain. Instead of assuming photo-consistency of 2D image intensities (the brightness constancy constraint does not hold, since the color of particles will change when they traverse different depth levels in axial direction), our 3D version of Horn-Schunck assumes a consistency on particle distribution fields $\mathbf{p}$ (see fourth term of Eq. (1)). In this way, the particle presence consistency term ties the particle and velocity reconstruction together into a joint optimization problem.

The described framework is also amenable to easily incorporating physical priors such as incompressibility of the fluid. In this work, we consider the fluids to be incompressible and nonviscous. One essential physical property for the incompressible fluids is mass conservation, which indicates zero divergence of the flow vectors. Additionally, the incompressible Navier-Stokes equation describes the time evolution of the fluid flows. These two physical priors account for the last two terms of Eq. (1). $\Pi_{\mathcal{C}_{\mathrm{DIV}}}$ is the operation to project arbitrary flow vector fields onto a space of divergence-free velocity field, $\mathbf{u}_{\mathrm{t}+1}(\mathbf{u}_{\mathrm{t}}, -\Delta t)$ and $\mathbf{u}_{\mathrm{t}-1}(\mathbf{u}_{\mathrm{t}-1}, \Delta t)$ approximate the time evolution of the flow vector fields backward and forward, respectively. Notice that we are not using the Navier-Stokes equations to compute the flows, but they are performed as regularization terms in the optimization problem (a variant of Horn-Schunck algorithm).

3.3 Depth Super-Resolution

The precedent RainbowPIV only delivers a limited and fixed depth levels because of the relatively low camera sensitivity to the wavelength change. This low depth resolution greatly limits its usage in many flow scenarios. The number of depth levels is dependent on the number of PSFs (each depth level has an unique PSF). In this work, we show that it is feasible to increase the number of PSFs by using a simple linear interpolation to generate in-between PSFs. We claim that the PSFs are not change linearly with respect to wavelength, while it is fair to assume that within a short wavelength range, the PSFs exhibit a linear change in approximation. It is worthy to point out that this super-depth strategy is not aiming to precisely locate the particles at particular depth level, otherwise, prompting to generate super-depth particle distribution fields with respect to the altered PSFs. With this simple digital adaptation (no hardware adjustment), we are able to reconstruct the flow vectors with super-resolved depth resolution. The accuracy of the reconstructed flow vectors in this fashion will be experimentally validated in the following.

4 Experimental Results

4.1 RainbowPIV and Tomo-PIV

A direct comparison of the RainbowPIV and Tomo-PIV is conducted under the simultaneous measurements. The depth of the measurement volume relies on the generated rainbow size. In the experiment, we work on a 25 *mm* rainbow with wavelength ranging from 480 *nm* to 680 *nm* (the rainbow size is easily adjustable by changing the distance of the employed two gratings). The size of the x-y plane observed by the camera is 50 $mm \times 35$ *mm*. The effective resolution of the captured RainbowPIV images is 1600×1120. We downsample the images by a factor of 8 in both dimensions (no further image preprocessing required), resulting in 200×140 images, and each particle occupies roughly 3×3 pixels. The particle seeding density is roughly 0.05 ppp (particle per pixel). The depth dimension is discretized into 100 levels in order to get regular voxel, where the PSFs of 20 levels (1.25 *mm* per level) are obtained by calibration, and the intermediate PSFs are digitally generated by linear interpolation based on the calibrated neighbor PSFs. Therefore, the reconstruction grid size is $200 \times 140 \times 100$. The pixel voxel ratio is 1:1:1 and the resolution for each voxel is approximately $0.25\ mm \times 0.25\ mm \times 0.25\ mm$. One vector per voxel will be generated by

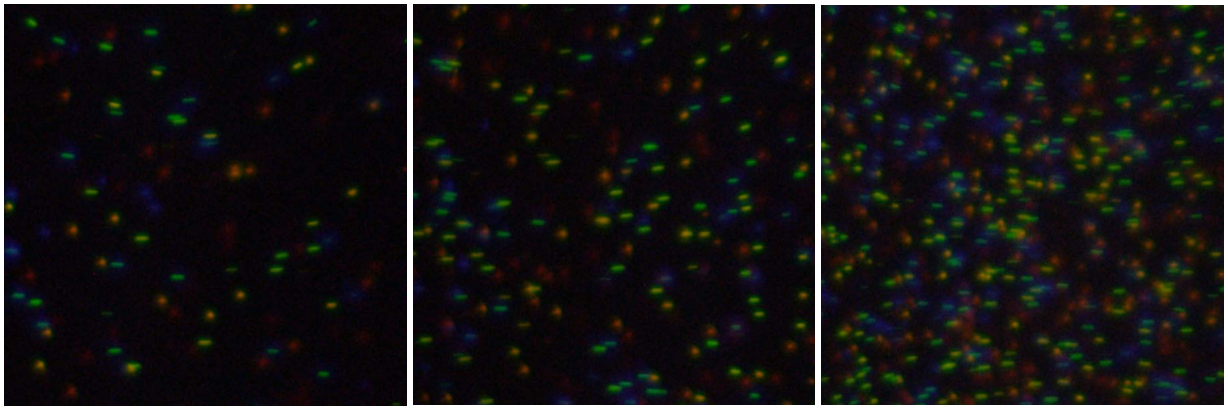

(a) (b) (c)

Figure 2: The captured RainbowPIV image with ppp = 0.005 (a), ppp = 0.015 (b) and ppp = 0.05 (c), respectively. Notice that with the employment of the specifically designed DOE, different colored particles have similar level of focus with the maximum aperture (f/1.8), even though they have different object distance.

the proposed algorithm, therefore, the reconstructed velocity field has the same dimension size and spatial resolution as the grids.

For the Tomo-PIV, a $1120 \times 780 \times 560$ particle intensity field is reconstructed by MART method, followed by a multi-pass cross-correlation with reduced interrogation window size and 75% overlap. The reconstructed velocity field has the size of $50 \times 35 \times 25$, resulting in a vector spatial resolution of $1\ mm \times 1\ mm \times 1\ mm$. All of the utilized algorithms are built in the LaVision Davis software.

A qualitative comparison of the reconstructed velocity fields for the introduced vortex ring at one time step is presented in Fig. 3. Two sliced views (one is perpendicular and the other is parallel to the image plane) of the reconstructed flow vectors and the color-coded vorticity magnitude are visualized. The overall flow structure obtained by RainbowPIV agrees well with that computed by Tomo-PIV, nevertheless, with multiple perspectives, Tomo-PIV has higher depth resolving capability than the proposed single view approach. We can observe that the reconstructed flow vectors from RainbowPIV in the depth direction exhibits to be more noisy compared with the flows in the image plane. As discussed in Sec. 3.3, on account of relatively lower sensitivity of the camera to the wavelength change, the camera is less sensitive to the particle motions in the axial direction than in-plane motions. Quantitative comparisons between Tomo-PIV and RainbowPIV show an average difference of about $0.05\ m/s$ for flow vector components in x-y plane and $0.1\ m/s$ for vector component in z direction with the maximum flow magnitude at $0.53\ m/s$. The uncertainty of the reconstructed axial flows are roughly twice that of the lateral flows. In comparison, in the original RainbowPIV work (Xiong et al., 2017), the axial uncertainty was roughly at six times the lateral uncertainty for an even narrower rainbow illumination, which confirms a dramatic axial resolution improvement.

Additional comparison is conducted by visualizing the isosurface of the velocity magnitude, as is shown in the top of Fig. 4. The figures reveal the high similarity of the core structures reconstructed by these two measurement technologies. We further verify the mass conservation properties of the reconstructed flow fields which should be complied with the physical property. The divergence of the computed flows is shown in the bottom of Fig. 4. Zero divergence is expected everywhere for incompressible fluids. This property is explicitly enforced by our reconstruction method, whereas the flow field from Tomo-PIV do not obey this physical property. This result demonstrates that, despite the overall high quality and detail of the Tomo-PIV solution, it can in fact *not* be considered a ground-truth solution.

4.2 Low Particle Seeding Density

Next, we evaluate the RainbowPIV system at low particle density situations, which are far below the desired particle density of Tomo-PIV. The correlation-based algorithms applied in Tomo-PIV require sufficiently dense seeding particles to extract accurate flow fields, and usually exhibits poor performance at low particle densities. The presented variant of optical flow method, however, eases the issue by exploiting a *local* constraint (particle presence consistency) which ensures that at those regions with present particles, the reconstructed *local* flow vectors match with the practical particle motion, and two *global* constraints (*global*

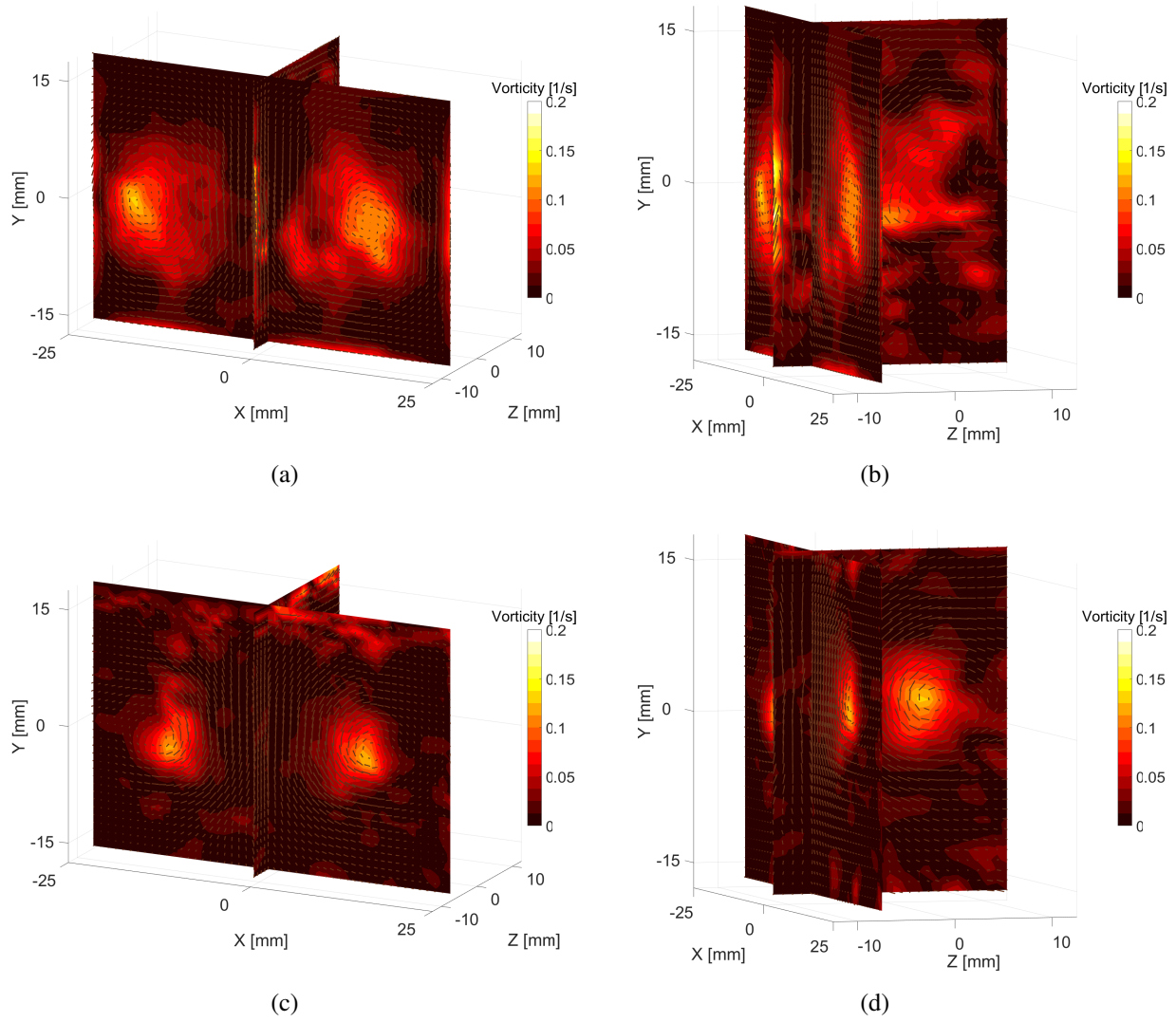

Figure 3: (a)-(b): Reconstructed flow vectors and vorticity magnitude by RainbowPIV; (c)-(d): Reconstructed flow vectors and vorticity magnitude by Tomo-PIV. The length of the arrow indicates the magnitude of the flow vectors. All the plots are in the same length scale.

smoothness constraint and temporal coherence) transmitting the accurate *local* flow vectors to the regions without particle presence. Moreover, the physical properties are always satisfied regardless of the particle density.

The tested particle seeding densities are roughly at 0.005 and 0.015 ppp, the captured images for which are shown in Fig. 2. The reconstructed flow vectors and vorticity magnitude are also visualized in Fig. 5, which demonstrates that RainbowPIV successfully captures the expected flow structures for the vortex ring at various low density levels. Owing to both of the *local* and the *global* constraints, the proposed method delivers decent results at rather low particle densities, under which conditions Tomo-PIV performs poorly. As a result, we believe that RainbowPIV can also be very competitive in experiments where uniform particle seeding is difficult or impossible.

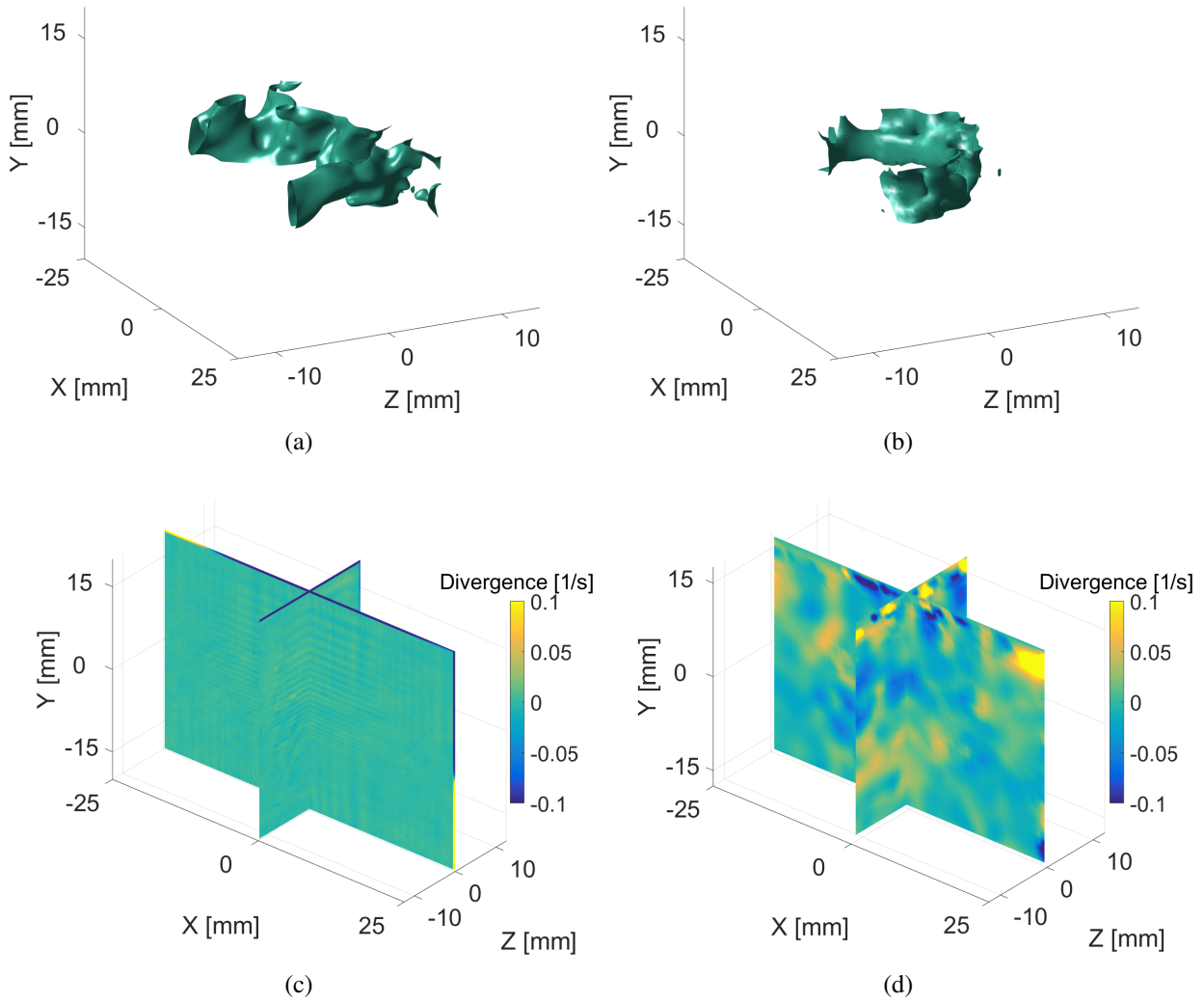

Figure 4: Isosurface visualization for the velocity fields computed from RainbowPIV (a) and Tomo-PIV (b); The divergence of the velocity fields ($\nabla \cdot \mathbf{u}$) by RainbowPIV (c) and Tomo-PIV (d).

5 Conclusion

In this paper, we have proposed a depth super-resolved RainbowPIV system which overcomes the limitation of axial resolution existed in precedent RainbowPIV system. A comprehensive study has been conducted for comparing the RainbowPIV with well developed four-camera Tomo-PIV using a simultaneous measurement setup. Both qualitative and quantitative results demonstrates a good agreement achieved by these two systems. Beyond the velocity consistency, owing to the physical-constrained velocity estimation model, RainbowPIV delivers divergence-free velocity fields for the measured incompressible fluids, whereas Tomo-PIV fails. In addition to that, with the employment of both local and global constraints, RainbowPIV successfully reconstructs velocity fields in rather low particle densities, which is restricted in Tomo-PIV. All the observations confirms the potential usage of RainbowPIV in 3D volumetric velocity measurements, specially in applications with limited optical access and low or non-uniform particle densities.

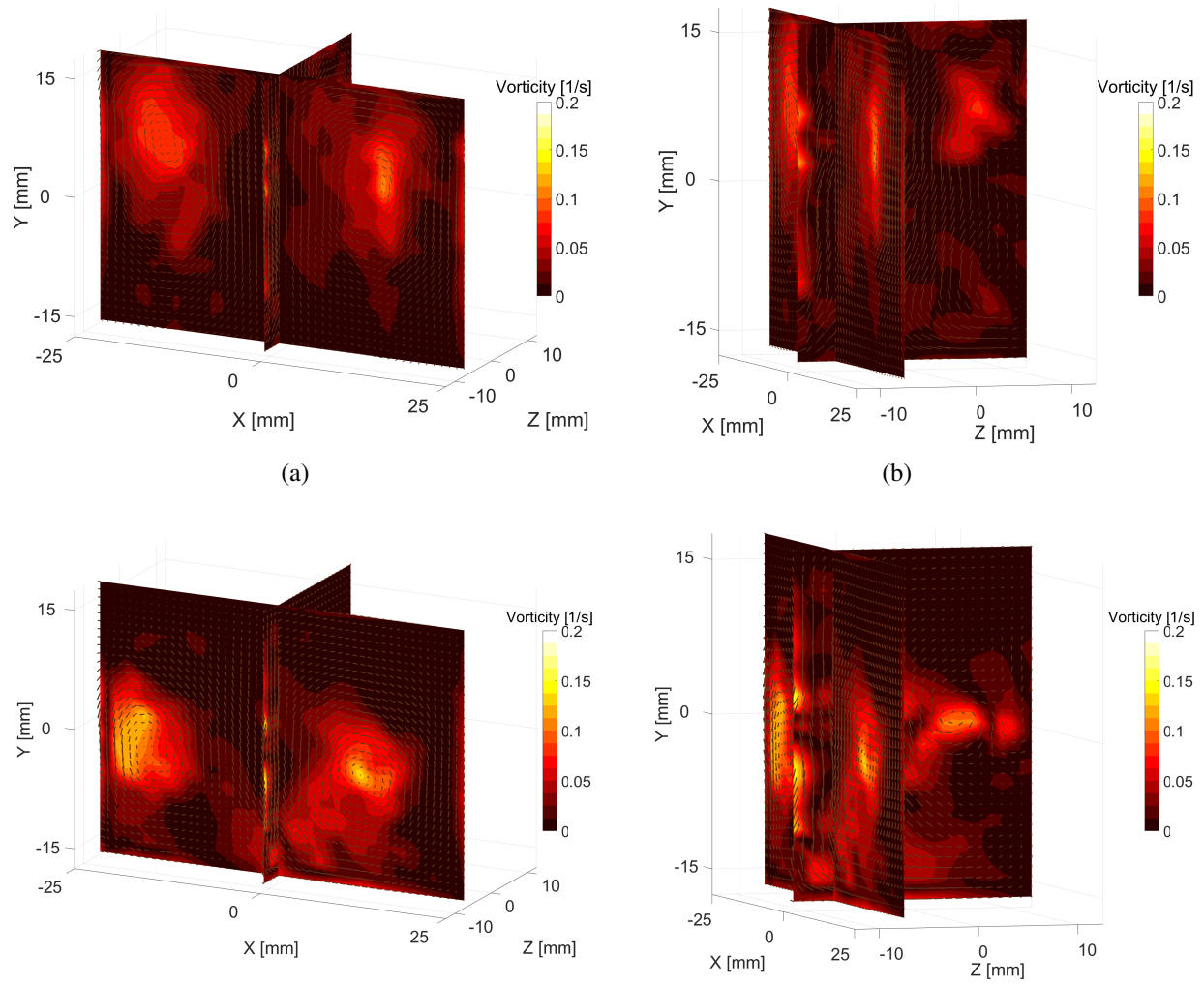

Figure 5: Reconstructed flow vectors and vorticity magnitude by RainbowPIV at ppp=0.005 (c)-(d) and ppp=0.015 (a)-(b).

Acknowledgements

This work was supported by King Abdullah University of Science and Technology through the CRG grant program as well as individual baseline funding.

References

Aguirre-Pablo A, Aljedaani A, Xiong J, Idoughi R, Heidrich W, and Thoroddsen S (2019) Single-camera 3d ptv using particle intensities and structured light. *Experiments in Fluids* 60:25

Aguirre-Pablo AA, Alarfaj MK, Li EQ, Hernández-Sánchez JF, and Thoroddsen ST (2017) Tomographic particle image velocimetry using smartphones and colored shadows. *Scientific Reports* 7:3714

Cierpka C, Hain R, and Buchmann NA (2016) Flow visualization by mobile phone cameras. *Experiments in Fluids* 57:108

Elsinga GE, Scarano F, Wieneke B, and van Oudheusden BW (2006) Tomographic particle image velocimetry. *Experiments in fluids* 41:933–947

Fahringer TW, Lynch KP, and Thurow BS (2015) Volumetric particle image velocimetry with a single plenoptic camera. *Measurement Science and Technology* 26:115201

Lasinger K, Vogel C, Pock T, and Schindler K (2018) 3d fluid flow estimation with integrated particle reconstruction. *40th German Conference on Pattern Recognition (GCPR 2018)*

Liu T, Merat A, Makhmalbaf M, Fajardo C, and Merati P (2015) Comparison between optical flow and cross-correlation methods for extraction of velocity fields from particle images. *Experiments in Fluids* 56:166

Liu T and Shen L (2008) Fluid flow and optical flow. *Journal of Fluid Mechanics* 614:253–291

McGregor T, Spence D, and Coutts D (2007) Laser-based volumetric colour-coded three-dimensional particle velocimetry. *Optics and lasers in engineering* 45:882–889

Pereira F and Gharib M (2002) Defocusing digital particle image velocimetry and the three-dimensional characterization of two-phase flows. *Measurement Science and Technology* 13:683

Prasad AK (2000) Particle image velocimetry. *CURRENT SCIENCE-BANGALORE-* 79:51–60

Rice BE, McKenzie JA, Peltier SJ, Combs CS, Thurow BS, Clifford CJ, and Johnson K (2018) Comparison of 4-camera tomographic piv and single-camera plenoptic piv. in *2018 AIAA Aerospace Sciences Meeting*. page 2036

Scarano F (2012) Tomographic piv: principles and practice. *Measurement Science and Technology* 24:012001

Scarano F and Moore P (2012) An advection-based model to increase the temporal resolution of piv time series. *Experiments in fluids* 52:919–933

Schanz D, Gesemann S, and Schröder A (2016) Shake-the-box: Lagrangian particle tracking at high particle image densities. *Experiments in fluids* 57:70

Schneiders JF and Scarano F (2016) Dense velocity reconstruction from tomographic ptv with material derivatives. *Experiments in fluids* 57:139

Shi S, Ding J, Atkinson C, Soria J, and New T (2018) A detailed comparison of single-camera light-field piv and tomographic piv. *Experiments in Fluids* 59:46

Shi S, Wang J, Ding J, Zhao Z, and New T (2016) Parametric study on light field volumetric particle image velocimetry. *Flow Measurement and Instrumentation* 49:70–88

Watamura T, Tasaka Y, and Murai Y (2013) Lcd-projector-based 3d color ptv. *Experimental Thermal and Fluid Science* 47:68–80

Willert C and Gharib M (1992) Three-dimensional particle imaging with a single camera. *Experiments in Fluids* 12:353–358

Xiong J, Fu Q, Idoughi R, and Heidrich W (2018) Reconfigurable rainbow piv for 3d flow measurement. in *2018 IEEE International Conference on Computational Photography (ICCP)*. pages 1–9. IEEE

Xiong J, Idoughi R, Aguirre-Pablo AA, Aljedaani AB, Dun X, Fu Q, Thoroddsen ST, and Heidrich W (2017) Rainbow particle imaging velocimetry for dense 3d fluid velocity imaging. *ACM Transactions on Graphics (TOG)* 36:36

Yoon SY and Kim KC (2006) 3d particle position and 3d velocity field measurement in a microvolume via the defocusing concept. *Measurement Science and Technology* 17:2897

Zang G, Idoughi R, Tao R, Lubineau G, Wonka P, and Heidrich W (2018) Space-time tomography for continuously deforming objects. *ACM Transactions on Graphics (TOG)* 37:100